Ultrasound Elasticity Imaging

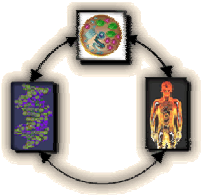

Stanislav (Stas) Emelianov
emelian@mail.utexas.edu

Department of Biomedical Engineering

THE UNIVERSITY OF TEXAS AT AUSTIN
THE UNIVERSITY of TEXAS HEALTH SCIENCE CENTER at HOUSTON
THE UNIVERSITY OF TEXAS MD ANDERSON CANCER CENTER Making Cancer History®

Outline

- Introduction
- Mechanical properties of tissue
- Approaches in elasticity imaging
- Elasticity imaging systems
- Applications
- Challenges, advantages and limitations
- Future developments

Notations

$X=(x_1,x_2,x_3)=(x,y,z)$ – coordinate system
$U=(u_1,u_2,u_3)$ – displacement vector
ε_{ij} – strain tensor $i=1,2,3$
σ_{ij} – stress tensor $j=1,2,3$

δ_{ij} – Kronecker delta
(1 for i=j, 0 otherwise)

Einstein summation convention –
summation is implied over the repeated index, for example:

$$a_{ii}=\sum_{i=1}^{3}a_{ii}=a_{11}+a_{22}+a_{33}$$

$$a_i b_{ij}=\sum_{i=1}^{3}a_i b_{ij} \quad \begin{aligned} j=1 &\rightarrow a_i b_{i1}=\sum_{i=1}^{3}a_i b_{i1}=a_1 b_{11}+a_2 b_{21}+a_3 b_{31} \\ j=2 &\rightarrow a_i b_{i2}=\sum_{i=1}^{3}a_i b_{i2}=a_1 b_{12}+a_2 b_{22}+a_3 b_{32} \\ j=3 &\rightarrow a_i b_{i3}=\sum_{i=1}^{3}a_i b_{i3}=a_1 b_{13}+a_2 b_{23}+a_3 b_{33} \end{aligned}$$

ρ – density (kg/m^3)

ν – Poisson's ratio
E – Young's modulus
λ, μ – Lame coefficients
G – shear modulus
K – bulk modulus
η – shear viscosity
ξ – bulk viscosity

c_t – shear wave speed
c_l – longitudinal wave speed

$$c_t=\sqrt{\frac{\mu}{\rho}},\quad c_l=\sqrt{\frac{\lambda+2\mu}{\rho}}$$

Elasticity Imaging – Goal

<u>Remote</u>
<u>non-invasive</u> (or adjunct to invasive)
<u>imaging</u> (or sensing) of
<u>mechanical properties</u> of
<u>tissue</u> for
<u>clinical</u> applications

Elasticity Imaging – Glance at History

Hippocrates, circa 460-377 B.C.

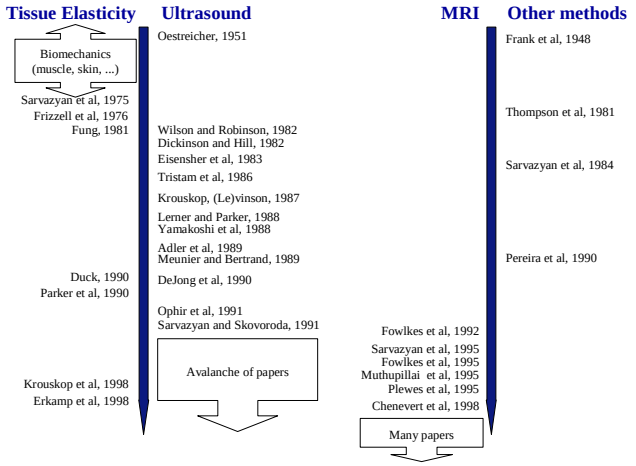

Mechanical Properties of Tissue (i.e., Why Bother)

Elasticity (e.g., bulk and shear moduli)

Viscosity (e.g., bulk and shear viscosities)

Nonlinearity (e.g., strain hardening)

Other (e.g., anisotropy, pseudoelasticity)

Elasticity

Changes in <u>tissue elasticity</u> are related to <u>pathological</u> changes

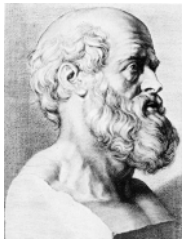

Hippocrates

… Such swellings as are <u>soft</u>, free from pain, and <u>yield to the finger</u>, ... and are <u>less dangerous</u> than the others.
... then, as are painful, <u>hard</u>, and large, indicate <u>danger of speedy death</u>; but such as are <u>soft</u>, free of pain, and <u>yield when pressed with the finger</u>, are more <u>chronic</u> than these.
THE BOOK OF PROGNOSTICS, Hippocrates, 400 B.C.

It is the business of the physician to know, in the first place, things similar and things dissimilar; … which are to be seen, <u>touched</u>, and heard; which are to be perceived in the sight, and the <u>touch</u>, and the hearing, … which are to be known by all the means we know other things.
ON THE SURGERY, Hippocrates, 400 B.C.

Hippocrates, 400 B.C.

Which Elastic Moduli?

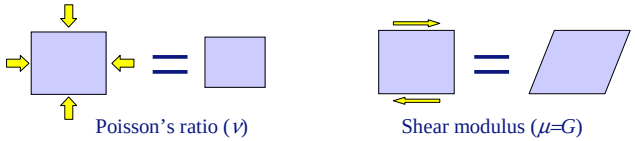

Poisson's ratio (ν)
Bulk modulus (K)

Shear modulus (μ=G)
Young's modulus (E)

Most soft tissues are incompressible, i.e., deformation produces <u>no</u> volume change

$$c_t = \sqrt{\frac{G}{\rho}} < c_l = \sqrt{\frac{K + \frac{2}{3}G}{\rho}} \rightarrow \boxed{G << K} \rightarrow \boxed{\frac{G}{K} \rightarrow 0} \rightarrow \boxed{\nu \rightarrow \frac{1}{2}}$$

Elasticity

Relations between various elastic constants

Constant	Common Pair		
	λ, μ	E, ν	K, G
λ	λ	$\frac{\nu E}{(1+\nu)(1-2\nu)}$	$K-\frac{2}{3}G$
μ	μ	$\frac{E}{2(1+\nu)}$	G
E	$\frac{\mu(3\lambda+2\mu)}{(\lambda+\mu)}$	E	$\frac{9KG}{3K+G}$
ν	$\frac{\lambda}{2(\lambda+\mu)}=0.5-\frac{\mu}{2(\lambda+\mu)}$	ν	$\frac{3K-2G}{6K+2G}$
K	$\lambda+\frac{2}{3}\mu$	$\frac{E}{3(1-2\nu)}$	K
G	μ	$\frac{E}{2(1+\nu)}$	G

Human sense of touch – what do we feel?

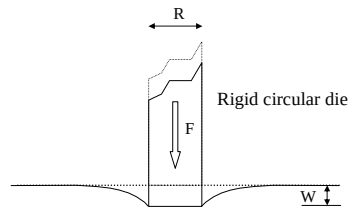

Semi-infinite elastic medium
K – bulk modulus
μ – shear modulus

Incompressible material

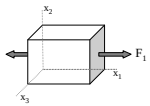

$$F_1 = 3\mu\varepsilon_0$$

$$F = 8RWG\left(1+\frac{\frac{G}{K}}{1+\frac{G}{3K}}\right)^{-1} \xrightarrow[\frac{G}{K}\to 0]{} 8RW\mu$$

Static deformation of (nearly) incompressible material is primarily determined by shear or Young's modulus (!!!), and boundary conditions (?!?)

Sarvazyan et al, 1995

How to (Directly) Measure Tissue Elasticity

- Sample preparation
- Deformation method
  - Static
  - Oscillatory (low frequency)
- Preconditioning of the tissue
- Load – Displacement measurements
- Strain – Stress calculations
- Elastic modulus evaluation

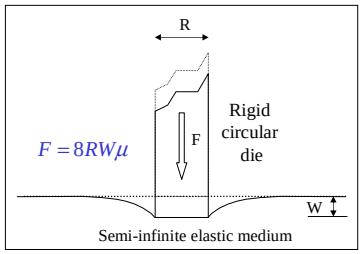

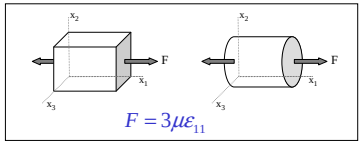

Direct Elasticity Measurements

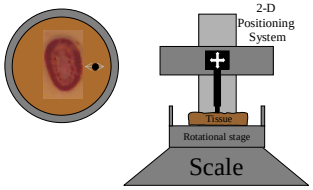

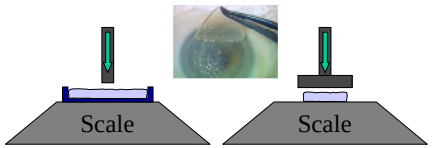

Load – Displacement Tests

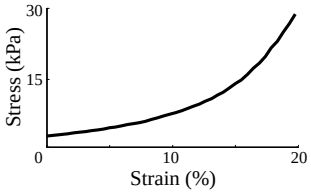

Erkamp et al, 1998

Direct Elasticity Measurements

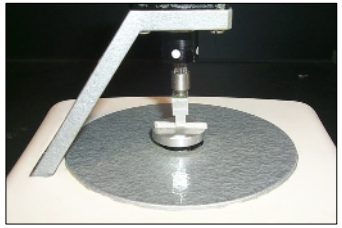

Artann Laboratories, NJ
www.artannlabs.com

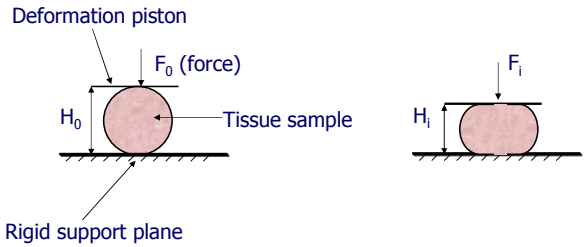

Artann Laboratories, NJ
Xie et al. 2004

Krouskop T.A., Wheeler T.M., Kallel F., Garra B.S., Hall T.J., "The elastic moduli of breast and prostate tissues under compression," *Ultrasonic Imaging,* 20:260-274, 1998.

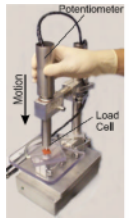

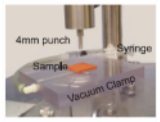

Wellman P.S., Howe R.D., Dalton E., Kern K.A., "Breast Tissue Stiffness in Compression is Correlated to Histological Diagnosis," Harvard BioRobotics Laboratory, Technical Report, 1999

Nava A., Mazza E., Haefner O., and Bajka M. "Experimental Observation and Modeling of Preconditioning in Soft Biological Tissues," *in Proceedings of Medical Simulation International Symposium, 2004 Cambridge*.

Samani A., Bishop J., Luginbuhl C. and Plewes D.B., "Measuring the elastic modulus of *ex vivo* small tissue samples," *Physics in Medicine and Biology*, 48, pp.2183-2198, 2003.

Breast Tissue Elasticity and Pathology

Skovoroda et al., 1995, *Biophysics,* 40(6):1359-1364.

Breast Tissue Type	Normal gland	Infiltrative ductal cancer with alveolar tissue predominating.	Fibroadenomas of glandular origin	Infiltrative ductal cancer with fibrous tissue predominating.	Ductal fibroadenoma
Young's Modulus (kPa)	**0.5-1.5**	**1.0-1.5**	**1.5-2.5**	**2.0-3.0**	**8.0-12.0**

Krouskop et al., 1998, *Ultrasonic Imaging*, 20:260-274.

Breast Tissue Type	**Tissue Elastic Modulus (kPa)**					
	5% precompression			**20% precompression**		
	Loading frequency (Hz)			**Loading frequency (Hz)**		
	0.1	1.0	4.0	0.1	1.0	4.0
Normal fat (n = 8)	18 ± 7	19 ± 7	22 ± 12	20 ± 8	20 ± 6	24 ± 6
Normal glandular tissue (n = 31)	28 ± 14	33 ± 11	35 ± 14	48 ± 15	57 ± 19	66 ± 17
Fibrous tissue (n = 18)	96 ± 34	107 ± 31	116 ± 28	218 ± 87	232 ± 60	244 ± 85
Ductal carcinoma *in situ* (n = 23)	22 ± 8	25 ± 4	26 ± 5	291 ± 67	301 ± 58	307 ± 78
Invasive and infiltrating ductal carcinoma (n = 32)	106 32	93 ± 33	112 ± 43	558 ± 180	490 ± 112	460 ± 178

Breast Tissue Elasticity and Pathology

Wellman et al., 1999, *Harvard BioRobotics Laboratory Technical Report.*

Tissue Type	Elastic Modulus at Strain 0.01	SD	Elastic Modulus at Strain 0.05	SD	Elastic Modulus at Strain 0.10	SD	Elastic Modulus at Strain 0.15	SD
Fat	4.8	2.5	6.6	7	10.4	7.9	17.4	8.4
Gland	17.5	8.6	33	12.0	88.1	66.7	271.8	167.7
Phyllodes Tumor	56.6	0.0	90.8	8.6	164.3	0.0	297.7	0.0
Papilloma	22.2	5.8	54.4	19.7	169.7	80.6	537.8	209.1
Lobular Carcinoma	34.7	0.0	78.9	0.0	221.8	0.0	628.4	0.0
Fibroadenoma	45.5	20.1	100.5	39.6	288.4	110.9	889.2	205
Infiltrating Ductal Carcinoma	47.1	19.8	115.7	42.9	384.5	126.9	1366.5	348.2
Ductal Carcinoma in Situ	71.2	0.0	188.7	0.0	638.7	0.0	2162.1	0.0

Samani et al., 2003, *Physics in Medicine and Biology*, 48:2183-2198

	Adipose tissue	Fibroglandular tissue	High grade ductal carcinoma
s (N m^{-1})	13.8	12.75	87.2
E (kPa)	1.9	1.8	12.0

Elastic Properties of Arteries

Sarvazyan A.P., 2001," *In: Handbook of Elastic Properties of Solids, Liquids and Gases.*

Type of soft tissue	E, kPa	Comments	Reference
Artery			
human, in vitro			
Thoracic aorta	300-940	For normal physiological conditions of longitudinal tension and distending blood pressure, below 200 mm Hg.	McDonald, 1974
Abdominal aorta	980-1,420		
Iliac artery	1,100-3,500		
Femoral artery	1,230-5,500		
Ascending aorta	183-582	M-mode echocardiography in different age groups.	Alessandri et al., 1995
Coronary artery	1,060-4,110	Represents values for various ages (0-80 y.o.) and atherosclerosis conditions in right and left arteries.	Ozolanta et al., 1998
rat, in vitro			
mesenteric small arteries	100-1,500	Equilibrated at intraluminal pressure of 45 mmHg, media thickness and lumen diameter were measured in the applied 3 -140 mmHg intraluminal pressure range.	Intengan et al., 1998
aortic wall	700-1,600	Range includes measurements for normal vs spontaneously hypertensive animals.	Marque et al., 1999
porcine, in vitro			
thoracic aorta			
intima-medial layer	43		
adventitia layer	4.7		
ascending aorta			
intima-medial layer	447	Bending experiments were used to impose various strains on different layers of tested blood vessels.	Fung, 1993
adventitia layer	112		
descending aorta			
intima-medial layer	248		
adventitia layer	69		

Elastic Properties of Prostate Gland

Aglyamov S.R. and Skovoroda A.R., 2000, *Biophysics, 2000, 45(6).*

Prostate gland

Canine prostate gland		Uniaxial compression		3–5	Parker et al. 1990
Human prostate gland				1–4	
	in normalcy			1–1.3	Skovoroda et al. 1995
Human prostate gland *in vitro*	1*	Indentation		1.3–1.5	
	2*			1.5–2.0	
	3*			2.3–3.0	
	4*			3.4–3.7	
	5*			3.7–4.5	
	central zone	NMR measurement of shear wave velocity	100 Hz	~18	Dresner et al. 1999
			300 Hz	~60	
			500 Hz	~130	
	peripheral zone		100 Hz	~8	
			300 Hz	~24	
			500 Hz	~65	
	front part in normalcy	Impedance measurements (frequency 0.1–4 Hz)		55 ± 14	Krouskop et al. 1998
	hinder part in normalcy			62 ± 19	
	benign hyperplasia			38 ± 8	
	cancer tumor			96 ± 19	

1* Adipose tissue.
2* Ulcerous nodes.
3* Cystically degenerated nodes.
4* Connective tissue membranes of nodes.
5* Hard nodes.

Contrast in Elasticity Imaging

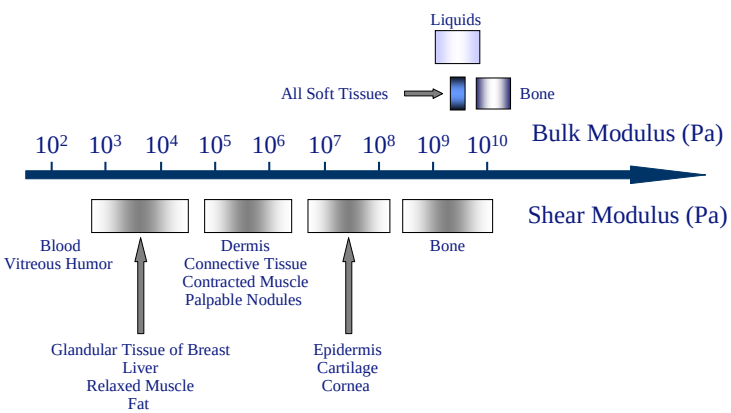

Sarvazyan et al, 1995

Strain hardening

- Most soft tissues exhibit strain hardening
- Tissues of organs with primary "mechanical" functions (muscle, skin, tendon, etc.)
- Other tissues (kidney, brain, blood clot, etc.)
- Strain hardening vs. strain softening (strain energy density function)

Vessel Composition (Fung, 1988):
muscle (soft), elastin (soft), collagen (hard)

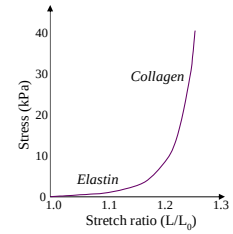

Strain hardening in kidney samples
(Erkamp et al, 1998)

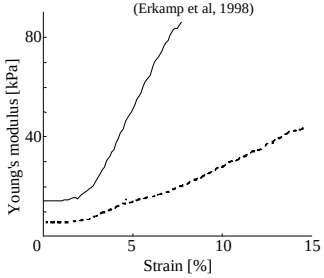

Strain hardening

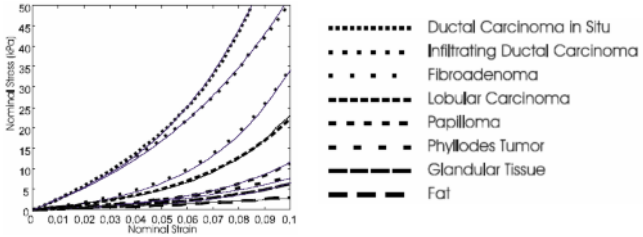

		Ratio to Fat at		
Tissue Type	Strain = 0.01	Strain = 0.05	Strain = 0.10	Strain = 0.15
Gland	4	5	8	16
Phyllodes Tumor	12	14	16	17
Papilloma	5	8	16	31
Lobular Carcinoma	7	12	21	36
Fibroadenoma	9	15	28	51
Infiltrating Ductal Carcinoma	10	18	37	79
Ductal Carcinoma in Situ	15	29	61	124

Table 4: The ratio of elastic modulus of each tissue type to fat at 4 different strain levels.

Wellman et al., 1999

Strain hardening

This and other graphs as well as other literature data suggest that tissue strain hardening (or nonlinearity in stress-strain relations) can be used for tissue analysis including composition, differentiation, etc.

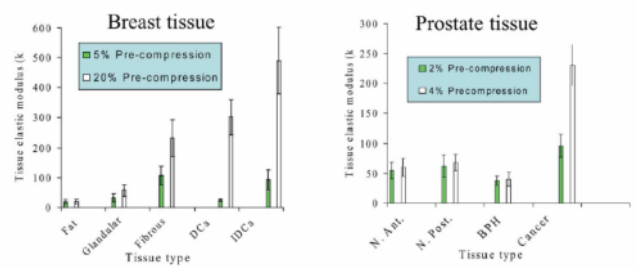

Figure 1. Tissue elastic moduli obtained from normal and abnormal breast and prostate tissues [26]. DCa = ductal carcinoma, IDCa = intraductal carcinoma, N. Ant. = anterior portion of the normal prostate, N. Post. = posterior portion of the normal prostate, BPH = benign prostatic hypertrophy.

Krouskop et al, 1998
Ophir et al., 2001

Anisotropy

- Arterial wall: orthotropic material – 9 constants
  two orthogonal planes of symmetry
- Muscle: transversely isotropic – 5 constants
  axis of symmetry
- Isotropic – 2 constants

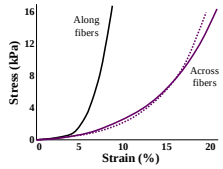

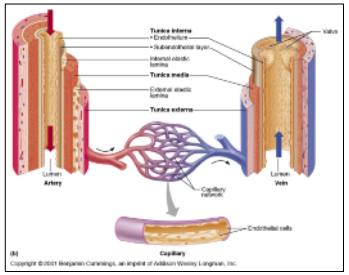

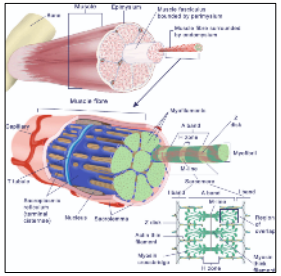

Viscosity

- Shear viscosity: shear waves
- Bulk viscosity: longitudinal ultrasound waves
- Viscoelastic models:
  Maxwell, Voigt, Kelvin, KVFD, etc.
- Is there a characteristic time?

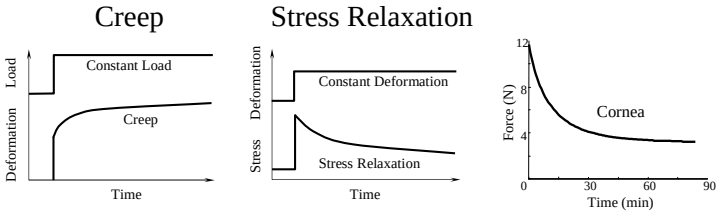

Viscosity

- Hysteresis loops:
  independent of the rate of loading (most soft tissues)
- Pseudoelastic material:
  elastic after preconditioning (with hysteresis)

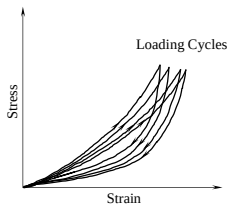

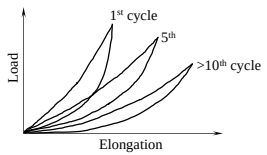

Mechanical Properties of Tissue: References

- Duck, F.A. Physical properties of tissues. Academic press; New York, 1990
- Fung YC. Biomechanics – mechanical properties of living tissues. Springer-Verlag; New York, 1981
- Krouskop TA, Wheeler TM, Kallel F, Garra BS, Hall TJ, "The elastic moduli of breast and prostate tissues under compression," *Ultrasonic Imaging* vol. 20 pp. 260-274, 1998
- Aglyamov SR, Skovoroda AR, "Mechanical properties of soft biological tissues," Biophysics, Pergamon, 45(6):1103-1111, 2000.
- Sarvazyan AP, "Elastic properties of soft tissues," In: Handbook of Elastic Properties of Solids, Liquids and Gases, Volume III, Chapter 5, 107-127, eds. Levy, Bass and Stern, Academic Press, 2001
- Other text books and archival publications

Phantoms for Elasticity Imaging

- Tissue-mimicking phantoms
  - Gelatin gels
  - Agar-agar and gelatin mixtures
  - Rubber (plastisol, silicone) materials
  - PVA (poly-vinyl alcohol)
  - Polyacrilamyde gels
- Tissue-containing phantoms
  - Gelatin gels
  - Agar-agar and gelatin gels
  - Polyacrilamyde gels

- Gelatin and Gelatin/Agar-agar
  - Easy to prepare
  - $E \sim C^n$, C – concentration, n=[1-2]
  - Short shelf life
  - Additives are possible
- Plastisol
  - Time-stable phantoms
  - Requires excessive heating during preparation
- PVA
  - Freeze-thaw cycles to vary elasticity
  - Time-stable

Hall et al., 1997
Other papers

Phantoms for Elasticity Imaging: Preparation

- PVA (poly-vinyl alcohol) tissue-mimicking phantom
- Background:
  8% PVA solution
  1% silica (40μm diameter)
  1 freeze/thaw cycle
- Inclusion:
  10% PVA solution
  2% silica particles
  3 freeze/thaw cycles
- Imaging:
  SONIX RP imaging system (Ultrasonix, Inc.)
  5-7 MHz, 40 mm linear probe
- Deformations
  manual
  0.3%

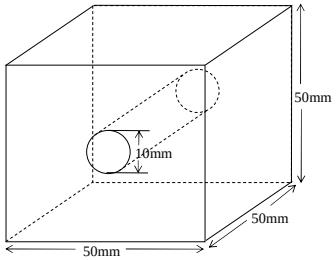

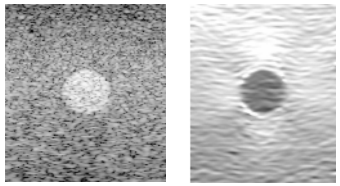

Park et al., 2007

29

Phantoms for Elasticity Imaging: References

- Madsen EL, Frank GR, Krouskop TA, Varghese T, Kallel F, Ophir J, "Tissue-mimicking oil-in-gelatin dispersions for use in heterogeneous elastography phantoms," *Ultrasonic Imaging* vol. 25 pp. 17-38, 2003
- Madsen EL, Hobson MA, Frank GR, Shi H, Jiang J, Hall TJ, Varghese T, Doyley MM, Weaver JB, "Anthropomorphic breast phantoms for testing elastography systems," *Ultrasound Med Biol.* vol. 32 pp. 857-874, 2006
- Hall TJ, Bilgen M, Insana MF, Krouskop TA, "Phantom materials for elastography," *IEEE Trans. UFFC*, vol. 44 pp. 1355-1365, 1997
- Surry KJM, Austin HJB, Fenster A, Peters TM, "Poly(vinly alcohol) cryogel phantoms for use in ultrasound and MR imaging," *Phys. Med. Biol.*, vol. 49 pp. 5529-5546, 2004
- Other text books and archival publications

- Where to buy
  ATS Laboratories, Inc. (http://www.atslabs.com/)

30

Elasticity Imaging using ...?

Computerized Tomography:
spatial distribution of the absorption (density)

MRI:
proton spin density and relaxation time constants

Ultrasound Imaging:
variation in acoustical impedance
(bulk modulus and density)

Optical Imaging:
refraction index

31

Elasticity Imaging – Approaches

Static (strain-based, or reconstructive)
imaging internal motion under static deformation

Dynamic (wave-based)
imaging shear wave propagation

Mechanical (stress-based, also reconstructive)
measuring tissue response at the surface

32

How … Static Elasticity Imaging?

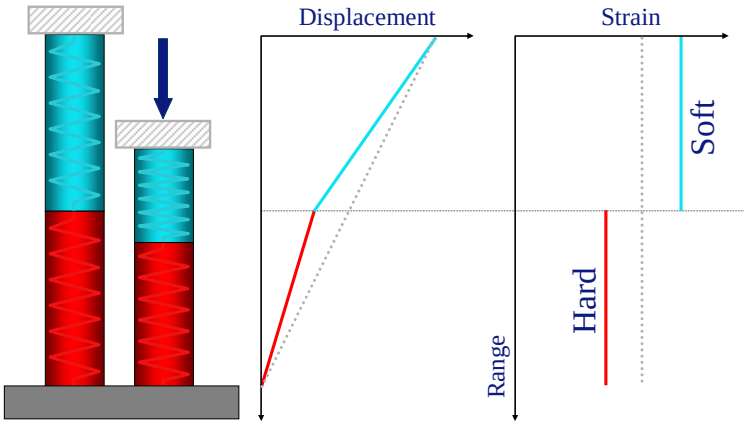

33

How … Static Elasticity Imaging?

- Capture data during deformation
- Estimate displacements
- Compute strain tensor
- Reconstruct mechanical properties

34

Elasticity Imaging – Main Components

- Capture data during externally or internally applied tissue motion or deformation
- Evaluate tissue response (displacement, strain, stress)
- Reconstruct elastic modulus based on theory of elasticity

Theory of elasticity is common part in all approaches in Elasticity Imaging

35

Theory of Elasticity (Static Approach)

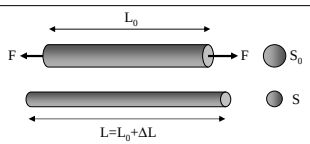

- Strain

$$\varepsilon_{11} = \frac{L - L_0}{L_0}$$

- Stress

$$\sigma_{11} = \frac{F}{S}$$

- Constitutive relationships

$$\sigma_{11} = E\varepsilon_{11} \qquad \text{E – Young's modulus}$$

- Equations of equilibrium

$$\frac{\partial \sigma_{11}}{\partial x_1} = 0$$

General (3-D) case

$$\varepsilon_{ij} = \frac{1}{2}\left(\frac{\partial u_i}{\partial x_j} + \frac{\partial u_j}{\partial x_i} + \frac{\partial u_k}{\partial x_i}\frac{\partial u_k}{\partial x_j}\right)$$

$$\Downarrow$$

$$\begin{pmatrix} \varepsilon_{11} & \varepsilon_{12} & \varepsilon_{13} \\ \varepsilon_{21} & \varepsilon_{22} & \varepsilon_{23} \\ \varepsilon_{31} & \varepsilon_{32} & \varepsilon_{33} \end{pmatrix} \longleftrightarrow \begin{pmatrix} \sigma_{11} & \sigma_{12} & \sigma_{13} \\ \sigma_{21} & \sigma_{22} & \sigma_{23} \\ \sigma_{31} & \sigma_{32} & \sigma_{33} \end{pmatrix}$$

$$\Downarrow$$

$$\sigma_{ij} = \lambda\varepsilon_{ii}\delta_{ij} + 2\mu\varepsilon_{ij}$$

$$\Downarrow$$

$$\sum_i \frac{\partial \sigma_{ij}}{\partial x_j} + f_i = 0$$

36

Equations of Equilibrium

Small deformations of linear, isotropic (i.e., Hookean) material

$$\frac{\partial}{\partial x_1}(\lambda(\frac{\partial u_1}{\partial x_1} + \frac{\partial u_2}{\partial x_2} + \frac{\partial u_3}{\partial x_3})) + \frac{\partial}{\partial x_1}(2\mu\frac{\partial u_1}{\partial x_1}) + \frac{\partial}{\partial x_2}(\mu(\frac{\partial u_1}{\partial x_2} + \frac{\partial u_2}{\partial x_1})) + \frac{\partial}{\partial x_3}(\mu(\frac{\partial u_1}{\partial x_3} + \frac{\partial u_3}{\partial x_1})) + f_1 = 0$$

$$\frac{\partial}{\partial x_2}(\lambda(\frac{\partial u_1}{\partial x_1} + \frac{\partial u_2}{\partial x_2} + \frac{\partial u_3}{\partial x_3})) + \frac{\partial}{\partial x_1}(\mu(\frac{\partial u_2}{\partial x_1} + \frac{\partial u_1}{\partial x_2})) + \frac{\partial}{\partial x_2}(2\mu\frac{\partial u_2}{\partial x_2}) + \frac{\partial}{\partial x_3}(\mu(\frac{\partial u_2}{\partial x_3} + \frac{\partial u_3}{\partial x_2})) + f_2 = 0$$

$$\frac{\partial}{\partial x_3}(\lambda(\frac{\partial u_1}{\partial x_1} + \frac{\partial u_2}{\partial x_2} + \frac{\partial u_3}{\partial x_3})) + \frac{\partial}{\partial x_1}(\mu(\frac{\partial u_3}{\partial x_1} + \frac{\partial u_1}{\partial x_3})) + \frac{\partial}{\partial x_2}(\mu(\frac{\partial u_3}{\partial x_2} + \frac{\partial u_2}{\partial x_3})) + \frac{\partial}{\partial x_3}(2\mu\frac{\partial u_3}{\partial x_3}) + f_3 = 0$$

Examples (incompressible material)

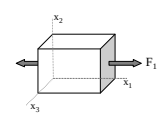

$$F_1 = 3\mu\varepsilon_0$$

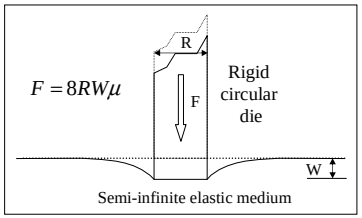

$$F = 8RW\mu$$

References

- Landau LD and Lifshitz EM. Theory of elasticity. Pergamon Press; New York, 1986
- Saada AS. Elasticity Theory and Applications. Krieger Publishing Company; Malabar, Florida, 1993
- Nowazki W. Dynamics of elastic systems. Wiley; New York, 1963
- Nowazki W. Thermoelasticity. Pergamon Press; New York, 1983
- Other text books and archival publications

Beware: most (soft) tissues are (nearly) incompressible

Image during Deformation

- Externally or internally induced deformation
- Continuous deformation while imaging
- Constrained or free-hand transducer
- Various imaging techniques
- Deformation, not translation

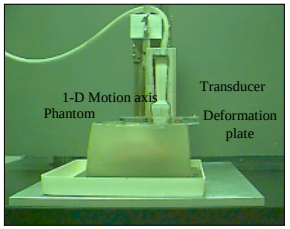

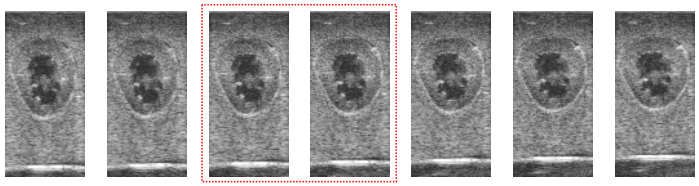

Displacements

- Speckle motion ↔ Tissue motion ↔ Speckle tracking
- Ultrasound Imaging (2-D → 3-D)
- Displacement vector: $U=(u_1,u_2,u_3)$
  - u_1 – lateral component
  - u_2 – axial (along the ultrasound beam)
  - u_3 – elevational (out-of-plane) component
- Various speckle tracking techniques
- "Anisotropy" in displacement measurements

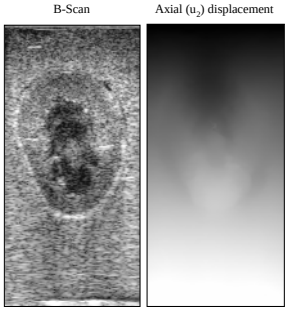

1-D, 2-D (3-D) Correlation Tracking

Normalized Correlation Coefficient

$$\hat{\rho}(l) = \frac{\int s_1^*(t)\cdot s_2(t+l)dt}{\sqrt{\int s_1^2(t)dt \cdot \int s_2^2(t+l)dt}}$$

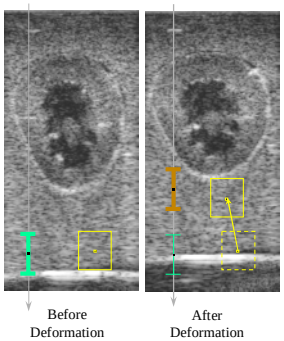

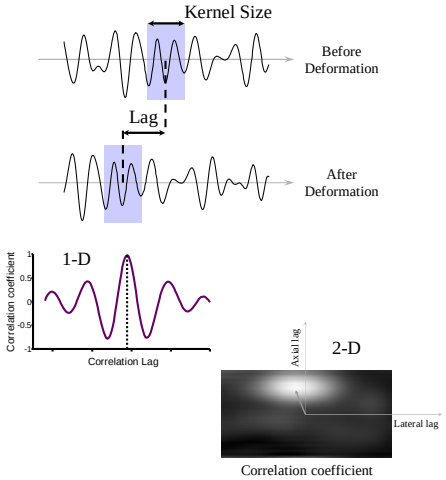

41

Strains

- Displacement vector → Strain tensor
- Displacement derivatives

$$\varepsilon_{ij} = \frac{1}{2}\left(\frac{\partial u_i}{\partial x_j} + \frac{\partial u_j}{\partial x_i} + \frac{\partial u_k}{\partial x_i}\frac{\partial u_k}{\partial x_j}\right)$$

- Six (3-D) or three (2-D) independent components

$$\begin{pmatrix} \varepsilon_{11} & \varepsilon_{12} & \varepsilon_{13} \\ \varepsilon_{21} & \varepsilon_{22} & \varepsilon_{23} \\ \varepsilon_{31} & \varepsilon_{32} & \varepsilon_{33} \end{pmatrix}$$

- Sources of error
- Improvement and Optimization
- Effect of strain hardening, anisotropy, etc.

Axial (u_2) displacement

Normal axial (ε_{22}) strain

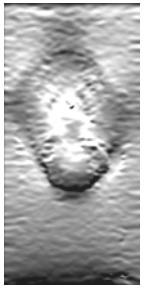

42

Static or Reconstructive Ultrasound Elasticity Imaging

B-Scan

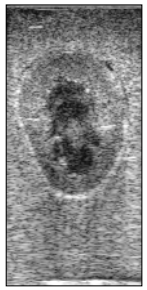

Deform and image

Displacements

Track internal motion

Strains

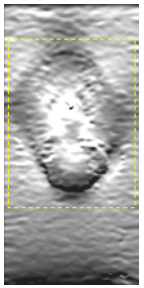

Evaluate deformations

Elasticity

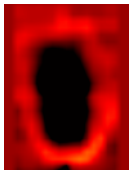

Reconstruct Young's or shear elastic modulus

43

Deformation: Challenges

Deformation vs. rotation and translation

translation – no information about tissue elasticity
rotation – no information about tissue elasticity and speckle tracking difficulties
deformation – consider "anisotropy" in displacement measurements (example 1)

Volumetric deformation vs. 1-D or 2-D US imaging

deformation – control the deformation state (i.e., plane strain) if possible

Deformation vs. temporal and spatial sampling

control deformation rate and/or frame rate and spatial sampling

Deformation vs. distribution and symmetries of elasticity

spatial symmetries (if any) must be considered to assist
displacement estimation
imaging of strain and interpretation (example 1 and 2)
elasticity reconstruction (example 1 and 2)

44

Strain Imaging: Challenges

Sources of error in strain images

ultrasound imaging system (electronic SNR, etc.)
interpolation
strain induced decorrelation
other sources (out-of-plane motion, peak hopping, etc.)

Optimal SNR and CNR in strain images

short-time correlation, companding, temporal stretching, strain filter, etc.
adaptive strain imaging for large deformations, multi-compression, etc.

Anisotropy in displacement measurements

incompressibility processing
other approaches (phase sensitive interpolation, grid slopes, etc.)

Effect of tissue strain hardening on strain images

utilize as independent parameter of tissue differentiation

A fundamental limit on delay estimation

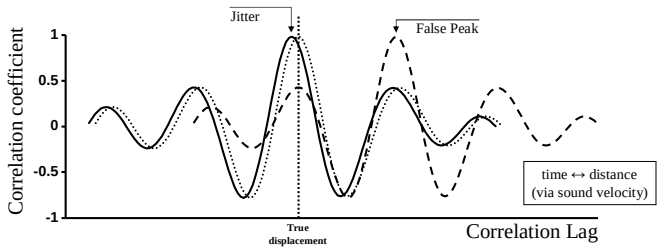

$$\sigma_\tau \geq \sqrt{\frac{3}{2 f_0^3 \pi^2 T\left(B^3+12B\right)}\left(\frac{1}{\rho^2}\left[1+\frac{1}{SNR^2}\right]^2-1\right)}$$

f_0 – center frequency
T – the observation time
B – fractional bandwidth

SNR – root mean squared signal-to-noise ratio
ρ – correlation coefficient
σ_τ – root mean squared time delay estimate error

Walker and Trahey, 1995

A fundamental limit on delay estimation

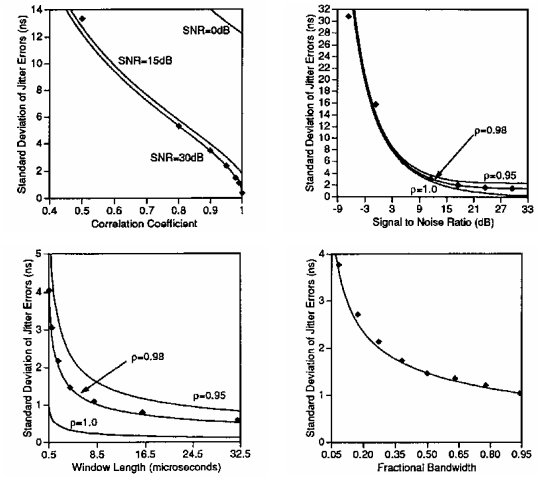

Walker and Trahey, 1995

Interpolation Error

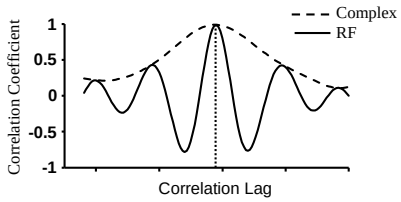

Two-step approach
(computationally efficient)

- Correlation peak position of complex baseband signal
- Phase zero-crossing of analytic signal correlation

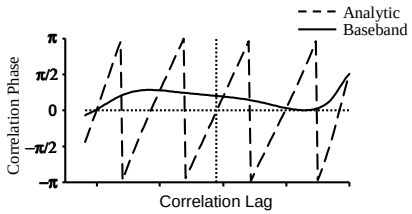

Some other approaches are discussed in:
Cespedes et al, 1995
Cohn et al, 1997
Pesavento et al, 1999
Geiman et al, 2000

O'Donnell et al, 1993
Lubinski et al, 1999

Strain Decorrelation

Strain → Decorrelation → Displacement Error → Strain Error

No strain

Displacement error ~ 1 / Kernel Size
(Kernel size ↔ Observation time ↔ Window size)

Strain decorrelation

Reduce kernel size

Filter correlation functions

Spatial resolution vs. error

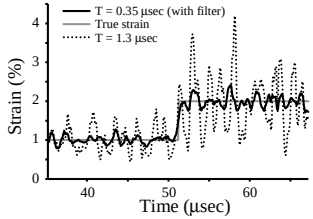

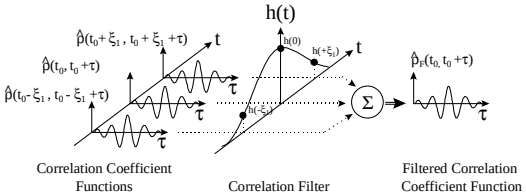

Lubinski et al, 1999

49

Time Delay Estimation and Interpolation Techniques

Time Delay Estimation
- Doppler-based techniques
- Optical Flow
- Normalized Covariance
- Normalized Cross-correlation
- Hybrid-sign Correlation
- Polarity-coincidence Correlation
- Cross-correlation
- Sum of Squared Differences (SSD)
- Sum of Absolute Differences (SAD)
- Mutual Information
- Many, many other algorithms

Interpolation
- Parabolic
- Phase zero crossing
- Cosine
- Spline
- Grid slopes
- Autocorrelation

Lubinski et al, 1999

50

Kernel size vs. resolution and SNR

Resolution

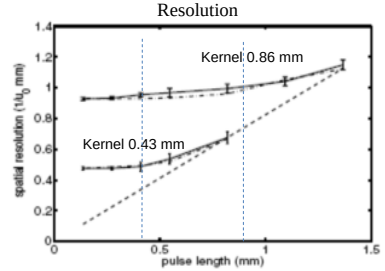

SNR

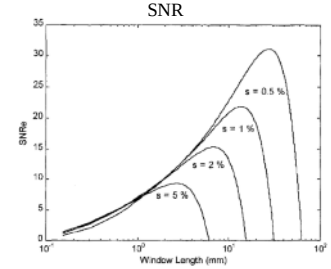

- Correlation window is longer than pulse length: the axial resolution of elasticity imaging is determined by the correlation window.
- Correlation window decreases to pulse length and below: spatial resolution is ultimately limited by the bandwidth of the ultrasonic imaging system.

$$T_{\text{opt}} \cong \frac{3B}{2s f_0^2}$$

Formula for optimal kernel size:
- B – bandwidth
- s – strain
- f_0 – center frequency

Liu et al., 2003

Varghese et al., 1998

51

Elasticity Imaging – Approaches

Static (strain-based, or reconstructive)
imaging internal motion under static deformation

Dynamic (wave-based)
imaging shear wave propagation

Mechanical (stress-based, also reconstructive)
measuring tissue response at the surface

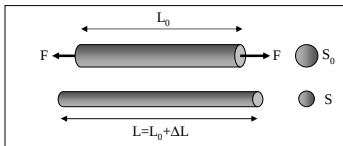

- Strain

$$\varepsilon_{11} = \frac{L - L_0}{L_0}$$

- Stress

$$\sigma_{11} = \frac{F}{S}$$

- Constitutive relationships

$\sigma_{11} = E\varepsilon_{11}$ E – Young's modulus

- Equations of motion

$$\frac{\partial \sigma_{11}}{\partial x_1} = \rho \frac{\partial^2 u_1}{\partial t^2}$$

52

Theory of Elasticity (Dynamic Approach)

General (3-D) case

$$\varepsilon_{ij} = \frac{1}{2}\left(\frac{\partial u_i}{\partial x_j} + \frac{\partial u_j}{\partial x_i} + \frac{\partial u_k}{\partial x_i}\frac{\partial u_k}{\partial x_j}\right)$$

$$\Downarrow$$

$$\begin{pmatrix} \varepsilon_{11} & \varepsilon_{12} & \varepsilon_{13} \\ \varepsilon_{21} & \varepsilon_{22} & \varepsilon_{23} \\ \varepsilon_{31} & \varepsilon_{32} & \varepsilon_{33} \end{pmatrix} \longleftrightarrow \begin{pmatrix} \sigma_{11} & \sigma_{12} & \sigma_{13} \\ \sigma_{21} & \sigma_{22} & \sigma_{23} \\ \sigma_{31} & \sigma_{32} & \sigma_{33} \end{pmatrix}$$

$$\Downarrow$$

$$\sigma_{ij} = \lambda \varepsilon_{ii}\delta_{ij} + 2\mu\varepsilon_{ij} + \xi \frac{\partial \varepsilon_{ii}}{\partial t}\delta_{ij} + 2\eta \frac{\partial \varepsilon_{ij}}{\partial t}$$

$$\Downarrow$$

$$\sum_i \frac{\partial \sigma_{ij}}{\partial x_j} + f_i = \rho \frac{\partial^2 u_i}{\partial t^2}$$

Example: plane waves

- Infinite homogeneous (λ,μ=const) elastic medium (i.e., ignore bulk and shear viscosities), no body forces (f_i=0)
- Assume that $u_1=u_1(x_1,t)$, $u_2=u_2(x_1,t)$, and $u_3=u_3(x_1,t)$

$$\frac{\partial}{\partial x_1}(\lambda(\frac{\partial u_1}{\partial x_1}+\frac{\partial u_2}{\partial x_2}+\frac{\partial u_3}{\partial x_3}))+\frac{\partial}{\partial x_1}(2\mu\frac{\partial u_1}{\partial x_1})+\frac{\partial}{\partial x_2}(\mu(\frac{\partial u_1}{\partial x_2}+\frac{\partial u_2}{\partial x_1}))+\frac{\partial}{\partial x_3}(\mu(\frac{\partial u_1}{\partial x_3}+\frac{\partial u_3}{\partial x_1}))=\rho\frac{\partial^2 u_1}{\partial t^2}$$

$$\frac{\partial}{\partial x_2}(\lambda(\frac{\partial u_1}{\partial x_1}+\frac{\partial u_2}{\partial x_2}+\frac{\partial u_3}{\partial x_3}))+\frac{\partial}{\partial x_1}(\mu(\frac{\partial u_2}{\partial x_1}+\frac{\partial u_1}{\partial x_2}))+\frac{\partial}{\partial x_2}(2\mu\frac{\partial u_2}{\partial x_2})+\frac{\partial}{\partial x_3}(\mu(\frac{\partial u_2}{\partial x_3}+\frac{\partial u_3}{\partial x_2}))=\rho\frac{\partial^2 u_2}{\partial t^2}$$

$$\frac{\partial}{\partial x_3}(\lambda(\frac{\partial u_1}{\partial x_1}+\frac{\partial u_2}{\partial x_2}+\frac{\partial u_3}{\partial x_3}))+\frac{\partial}{\partial x_1}(\mu(\frac{\partial u_3}{\partial x_1}+\frac{\partial u_1}{\partial x_3}))+\frac{\partial}{\partial x_2}(\mu(\frac{\partial u_3}{\partial x_2}+\frac{\partial u_2}{\partial x_3}))+\frac{\partial}{\partial x_3}(2\mu\frac{\partial u_3}{\partial x_3})=\rho\frac{\partial^2 u_3}{\partial t^2}$$

$$(\lambda+2\mu)\frac{\partial^2 u_1}{\partial x_1^2}-\rho\frac{\partial^2 u_1}{\partial t^2}=0 \rightarrow \frac{\partial^2 u_1}{\partial x_1^2}-\frac{1}{c_l^2}\frac{\partial^2 u_1}{\partial t^2}=0 \text{ where } c_l=\sqrt{\frac{\lambda+2\mu}{\rho}}$$

Longitudinal wave (ultrasound)

$$\mu\frac{\partial^2 u_{2(3)}}{\partial x_1^2}-\rho\frac{\partial^2 u_{2(3)}}{\partial t^2}=0 \rightarrow \frac{\partial^2 u_{2(3)}}{\partial x_1^2}-\frac{1}{c_t^2}\frac{\partial^2 u_{2(3)}}{\partial t^2}=0 \text{ where } c_t=\sqrt{\frac{\mu}{\rho}}$$

Shear wave

Transient Elastography

The displacement vector is not always orthogonal to the propagation vector:
finite medium, finite size vibrator
shear wave is not purely transverse

Transmit low frequency shear waves
mechanical vibration parallel to ultrasound beam

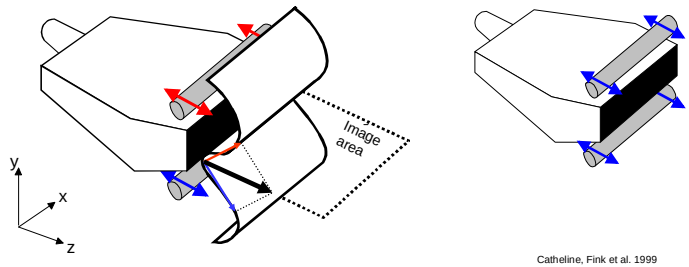

Catheline, Fink et al. 1999
Laboratoire Ondes et Acoustique, France
http://www.loa.espci.fr/

Transient Elastography

Image shear waves and measure its velocity using ultrafast imaging and motion tracking

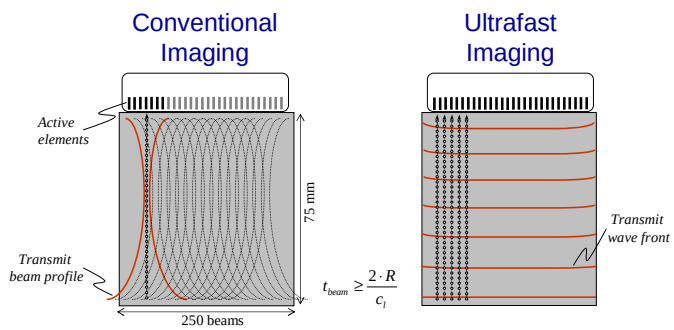

Time needed to acquire 1 frame:

$$t_{frame}=t_{beam}\cdot\#beams=\frac{2\cdot 75\,\text{mm}}{1.5\,\text{mm}/\mu\text{m}}\cdot 256\approx 25\,\text{ms}$$

$$t_{frame}=t_{beam}=\frac{2\cdot 75\,\text{mm}}{1.5\,\text{mm}/\mu\text{m}}\approx 100\,\mu\text{s}$$

Transient Elastography

Evaluate shear modulus from shear wave velocity

Isotropic, homogeneous, elastic medium

$$\rho\frac{\partial^2\vec{u}}{\partial t^2}=\underbrace{(\lambda+\mu)\vec{\nabla}(\vec{\nabla}.\vec{u})}_{\text{compression}}+\underbrace{\mu\vec{\Delta}\vec{u}}_{\text{shear}}$$

Shear wave propagation equation

$$\rho\frac{\partial^2 u_i}{\partial t^2}=\mu\Delta u_i \;,\quad i=x,y,z$$

Local inversion algorithm

$$V_s(x,z)=\sqrt{\frac{1}{N}\sum_{n=1}^{N}\frac{\partial^2 u(x,z,t)}{\partial t^2}\left(\frac{\partial^2 u(x,z,t)}{\partial x^2}+\frac{\partial^2 u(x,z,t)}{\partial z^2}\right)^{-1}}$$

57

Transient Elastography

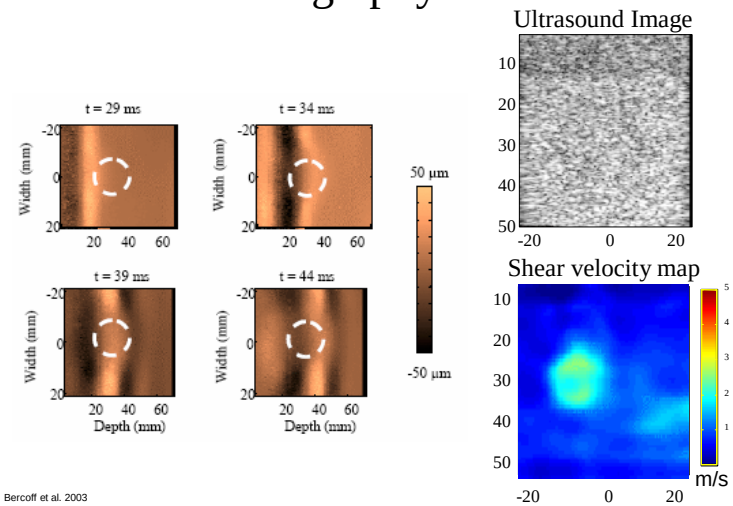

Bercoff et al. 2003

58

Acoustic Radiation Force Imaging

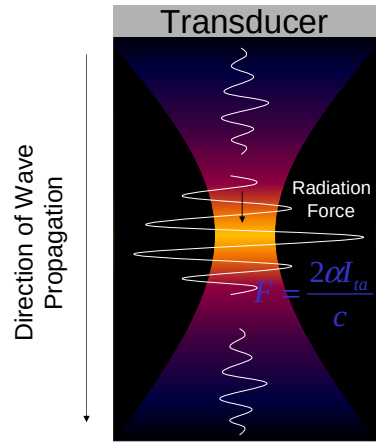

1. Focused Acoustic Radiation Force generates localized, impulsive (<0.1 ms) tissue excitation
2. Track tissue response with same ultrasonic transducer used for force generation
3. Repeat in multiple locations throughout 2D FOV
4. Generate images of relative tissue response within the region of excitation (displacement after force removal, recovery time, etc) to assess structural information about tissue

Nightingale, Trahey et al.
Duke University

Shear Wave Imaging

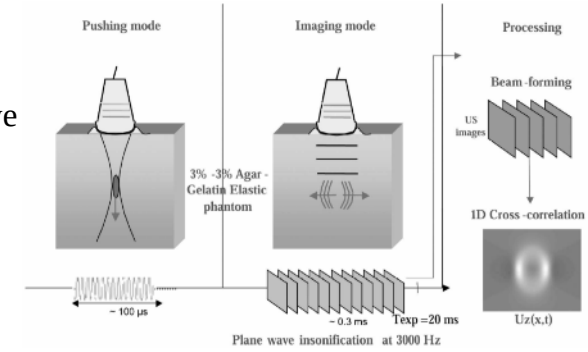

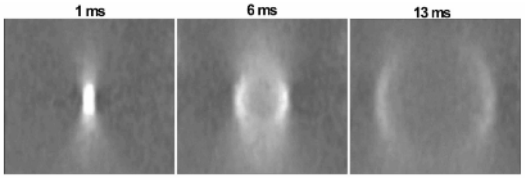

Bercoff et al. 2004

60

Supersonic Shear Wave Imaging

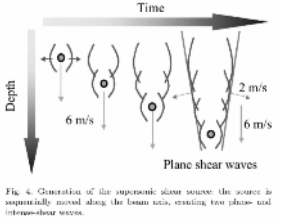

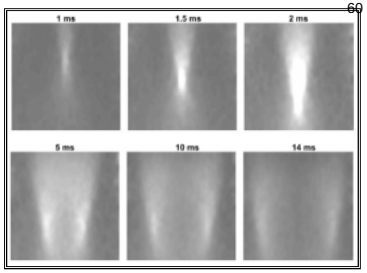

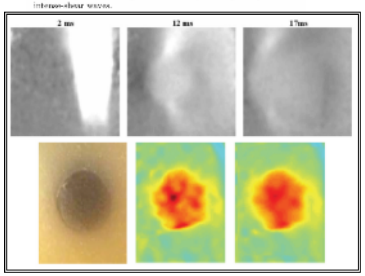

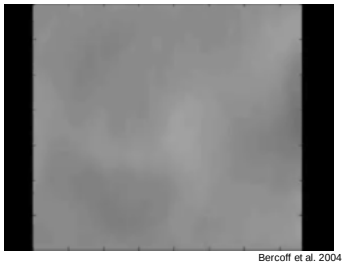

Bercoff et al. 2004

61

Elasticity Imaging Systems (Static / Dynamic)

- Siemens/Acuson Antares
- Hitachi Imaging System
- Sonic RP by Ultrasonix Medical, Inc.
- Volcano Therapeutics IVUS Imaging
- Winprobe Research Platform
- Other systems
- Supersonic Imaging, Inc.
- Siemens
- Echosens
- Other systems

62

Siemens Sonoline Elegra and Acuson Antares systems

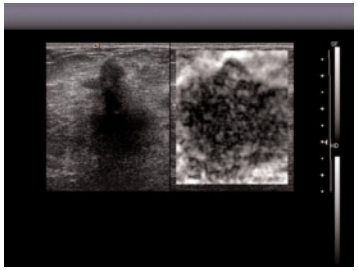

eSie Touch elasticity imaging
• Improves border delineation of this biopsy-proven invasive ductal carcinoma. Live dual imaging provides real time comparison of elastogram to standard 2D imaging.

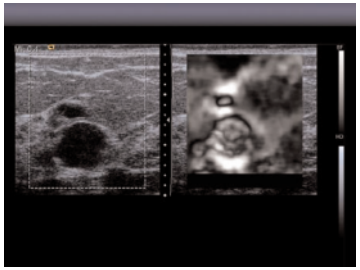

eSie Touch elasticity imaging
• Provides additional qualitative information by demonstrating the typical internal characteristics pattern of three cysts.

www.siemens.com

63

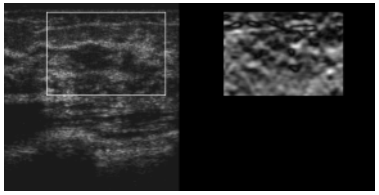

Fibroadenoma:
changing contrast
equal lesion size ratio

IDC:
constant contrast
large lesion size ratio

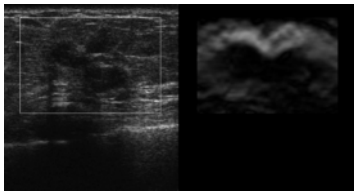

Hall et al, 2006
www.engr.wisc.edu/bme/faculty/hall_timothy.html
www.medphysics.wisc.edu/medphys_docs/people/hall/hall.html

64

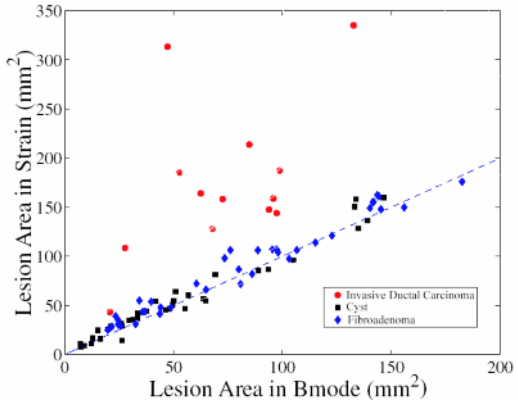

Hall, Zhu et al, 2003

Lesion size comparison technique

65

Benign fibroadenoma

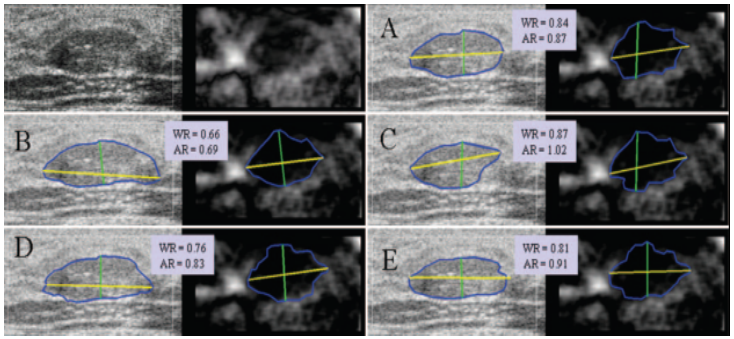

WR - size ratios for width
AR - size ratios for area

A, B, C, D, E – five observers

Regner et al. 2006

Lesion size comparison technique

66

Invasive ductal carcinoma

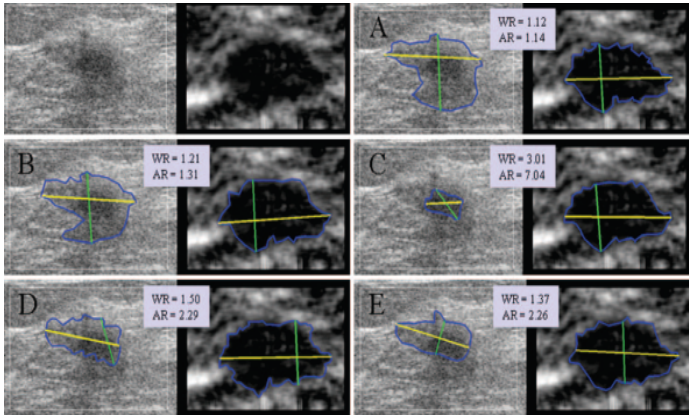

WR - size ratios for width
AR - size ratios for area

A, B, C, D, E – five observers

Regner et al. 2006

Lesion size comparison technique

67

Potential problems: for some lesions it is difficult to distinguish from the surrounding breast tissue on B-mode images.

Benign fat necrosis

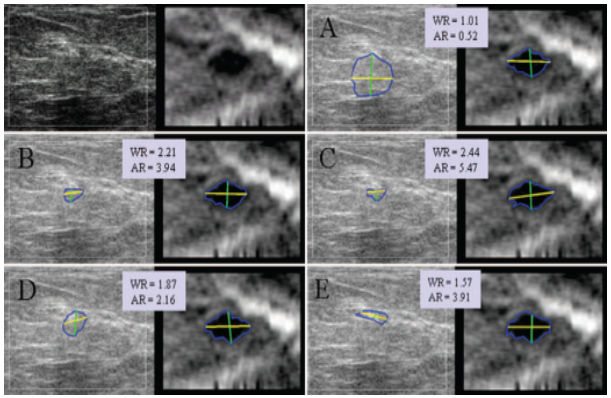

WR - size ratios for width
AR - size ratios for area

A, B, C, D, E – five observers

Regner et al. 2006

Lesion size comparison technique

68

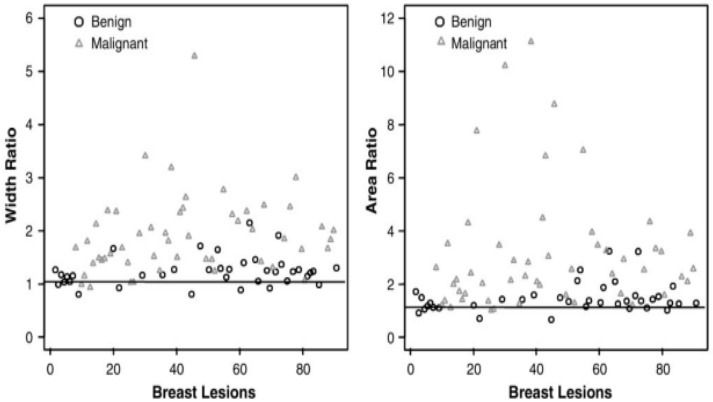

Regner et al. 2006

Hitachi HI Vision 8500/900 systems

69

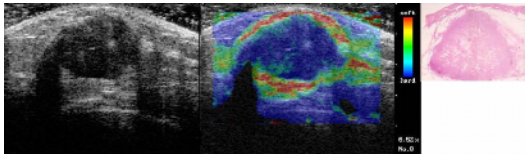

Nonscirrhous type invasive ductal carcinoma in 29-year-old woman

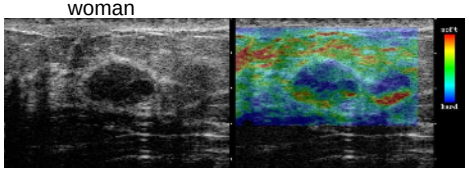

Fibroadenoma with in 39-year-old woman

HITACHI

Itoh et al. 2006

Acoustic Radiation Force Imaging: Breast

70

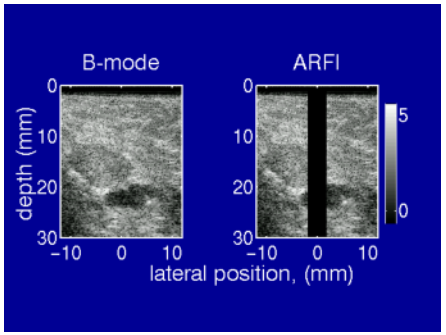

ARFI image of an in-vivo breast lesion (an infected lymph node) showing differences in displacement and recovery response of different tissues to radiation force excitation

Nightingale, Trahey et al.

In vivo Breast Lymph Node (Reactive, Benign)

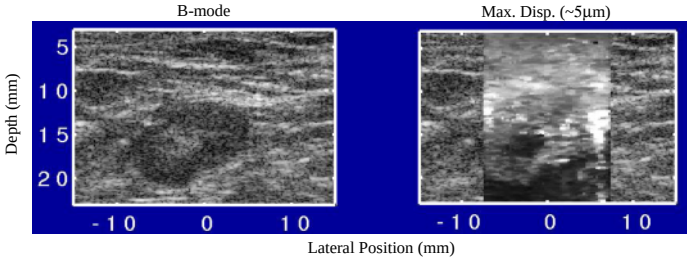

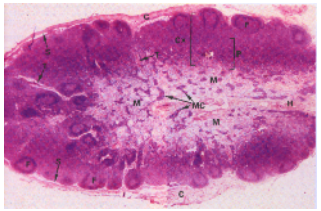

Typical Lymph Node Histology

Reproduced from Wheater's Functional Histology, 4th Ed.

Nightingale et al.; Trahey et al.
Duke University

In Vivo Breast Lesions

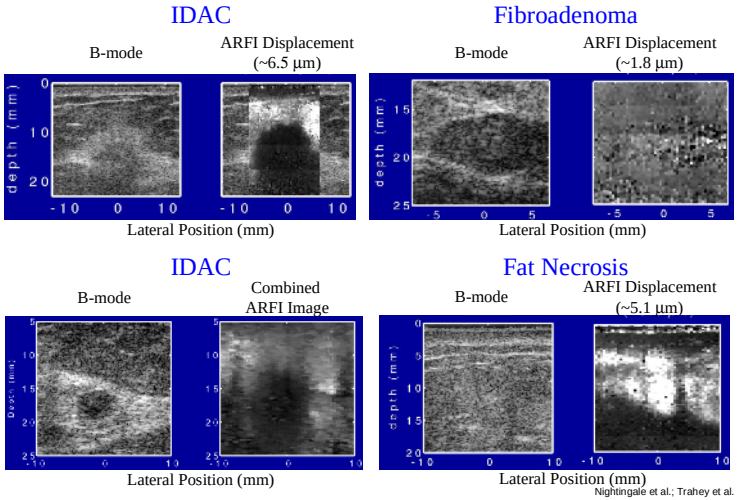

Nightingale et al.; Trahey et al.

73

Supersonic Imagine: Elasticity Imaging of Breast

74

Elasticity Imaging of Prostate cancer

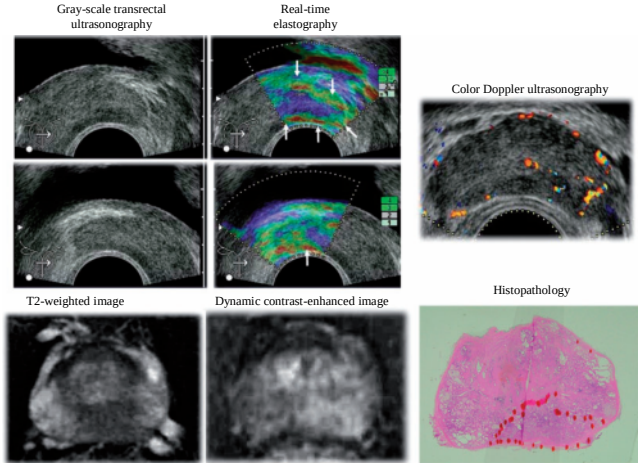

Sumura et al., 2007

75

Real-time (30 fps) Strain Imaging of Prostate: Digital System, 7.5 MHz

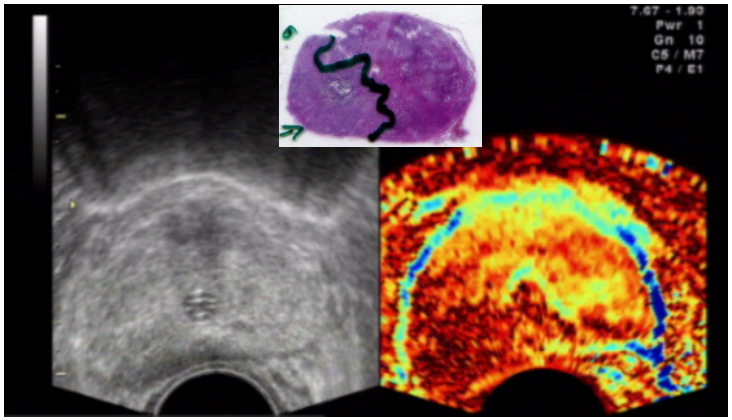

Ruhr Center of Competence for Medical Engineering
Bochum, Germany (http://www.hf.ruhr-uni-bochum.de)

76

Elastography of Thermal Lesions in the Liver after RF Ablation

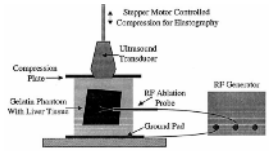

Fig. 1. Schematic diagram of the system used for radiofrequency ablation (RFA), probe guidance, and elastography. The RFA probe has four heating elements with thermosensors on the tip of each element. The ablation probe was inserted perpendicular to the scan plane of the US transducer.

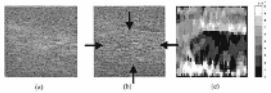

Fig. 4. B-mode grey-scale images and elastograms obtained from a lobe of liver tissue encased in a gelatin phantom; (a) a B-mode image before RFA, (b) a B-mode image after RFA. The melting of the gelatin above the liver sample, and a slight reduction in echogenicity in (b) are the only visible changes evident from RFA, and (c) illustrates the axial strain elastogram obtained on the ablated liver tissue using a 1% applied compression. Note the delineation of the ablated region (thermal lesion) from the surrounding tissue, due to the increased stiffness (low strain) in the ablated region.

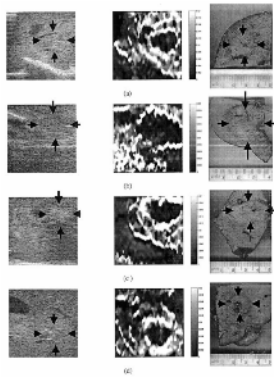

Fig. 6. *In vivo* (a)–(d) US B-mode images and elastograms along with gross-pathology photographs for the four thermal lesions generated in liver tissue. The elastograms shown illustrate the repeatability of our results. Note the clear elastographic depiction of the thermal lesions, with the stiffer necrotic core of the lesion surrounded by softer tissue that appears as the bright halo around the lesion. The lesion size depicted in the elastograms corresponds closely with the pathology photographs.

Varghese et al. 2002

Monitoring liver stiffness after RF ablation

77

Canine liver tissue *in vitro*

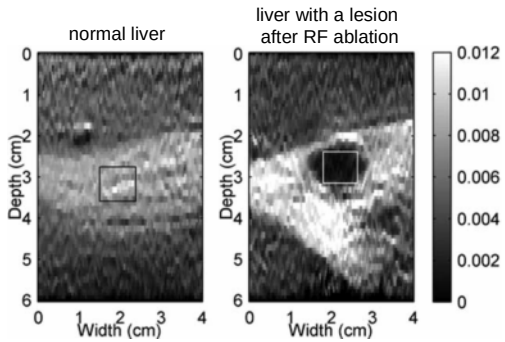

Bharat et al., 2005

Ex Vivo RF Liver Ablation

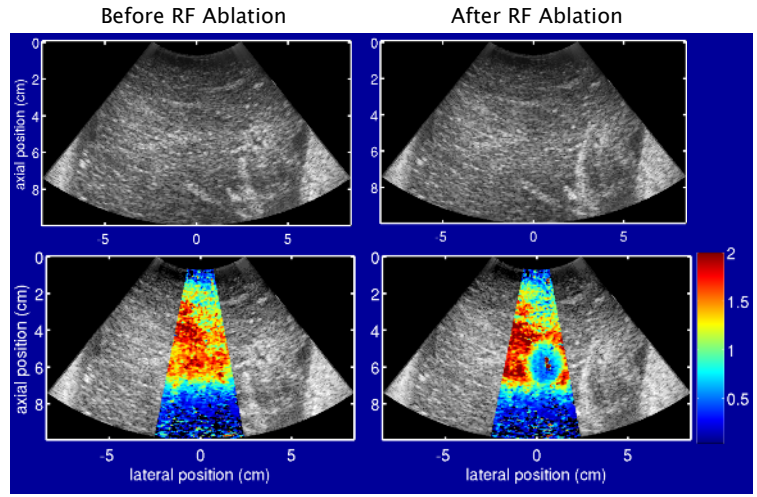

Nightingale et al.; Trahey et al.

Staging of Liver Fibrosis with Radiation Force

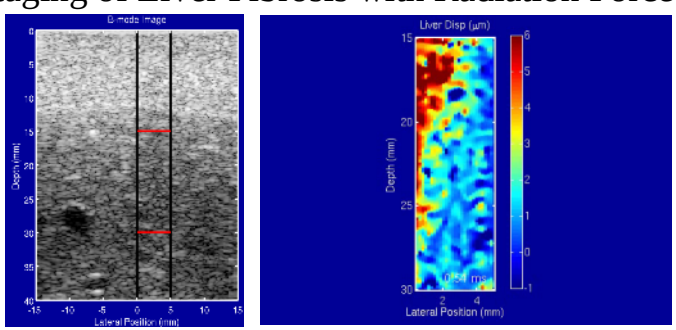

Key clinical question is degree to which liver fibrosis has occurred
Biopsy? Imaging?
Quantitative measure of liver stiffness is needed
SWEI: new shear wave speed estimation approach
eliminates 2nd order differentiation

Nightingale et al.; Trahey et al.

80

Fibroscan

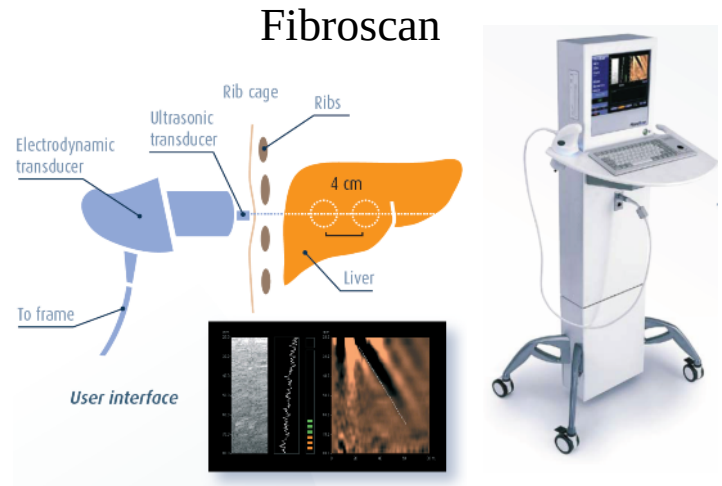

http://www.echosens.com

81

Non-invasive staging of liver fibrosis

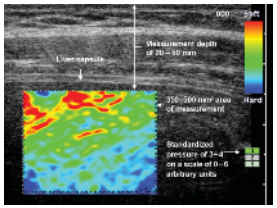

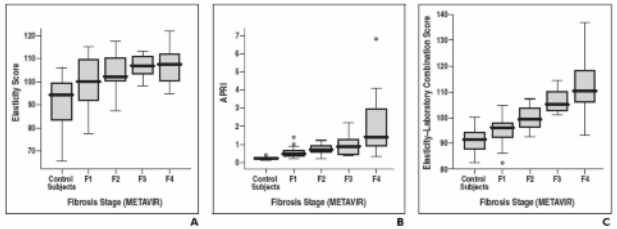

A. Real-time elastography; B. Aspartate transaminase-to-platelet ratio index; C. Elasticity- laboratory combination values

Friedrich-Rust et al. 2007

82

SuperSonic Imagine: ShearWave Elastography

In vivo assessment of Young's modulus in a healthy volunteer

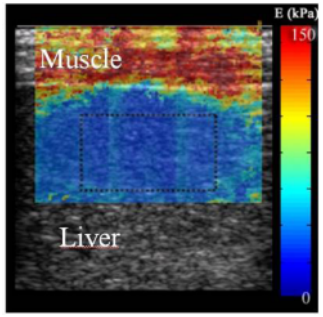

Deffieux at al. 2007

83

Ulrasonix Sonix RP Imaging System

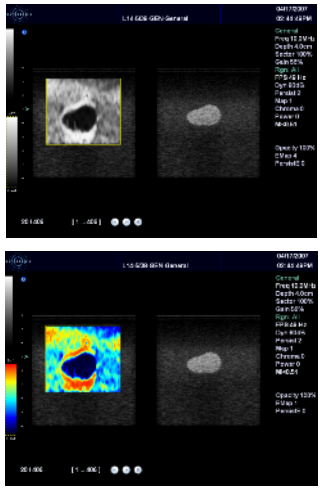

www.ultrasonix.com

84

Winprobe Elasticity Imaging System (FPGA-based solution)

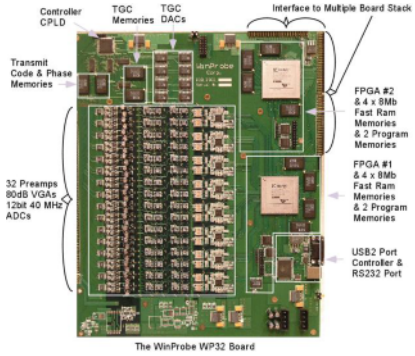

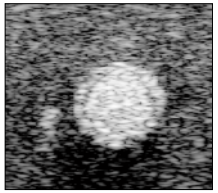

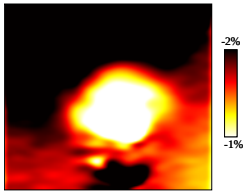

www.winprobe.com

85

Characterizing lesions - Palpograms

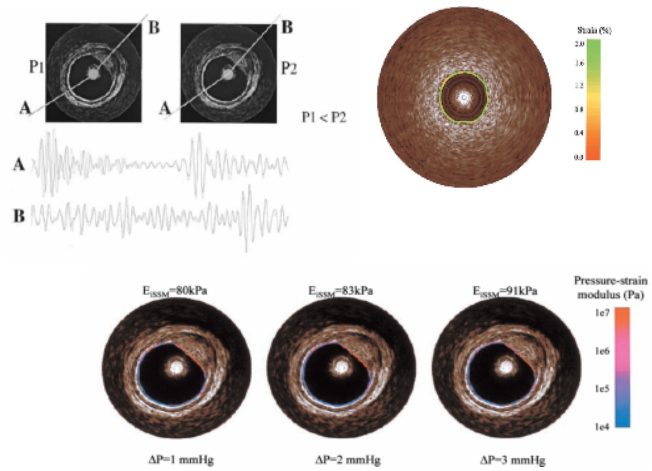

Cespedes, De Korte et al./Ultrasound in Med. & Biol., Vol. 26, No. 3, pp. 385–396, 2000

86

In vivo acquisition scheme

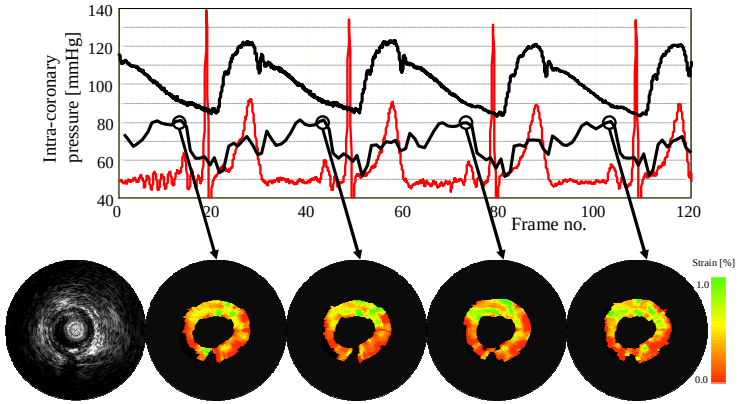

Eur Heart J 23(5): 405-413 (2002)

de Korte, Mastik and van der Steen
Erasmus Medical Center, Rotterdam
http://www.eur.nl/fgg/thorax/elasto/

87

3 Dimensional Elastography:
feasibility in a human coronary

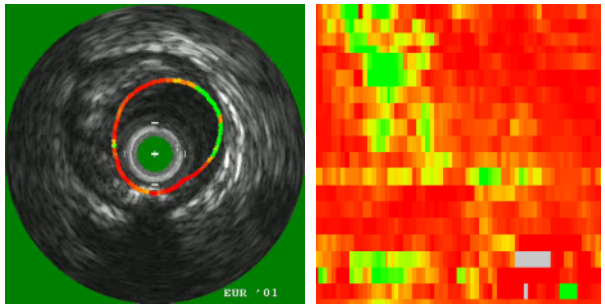

de Korte, Mastik and van der Steen
Erasmus Medical Center, Rotterdam
http://www.eur.nl/fgg/thorax/elasto/

88

Vascular Strain Imaging using Arterial Pressure Equalization

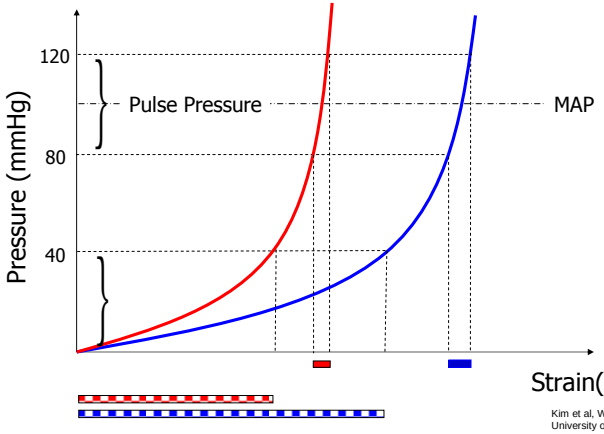

Kim et al, Weitzel et al
University of Michigan
http://bul.eecs.umich.edu/

89

Vascular Strain Imaging using Arterial Pressure Equalization

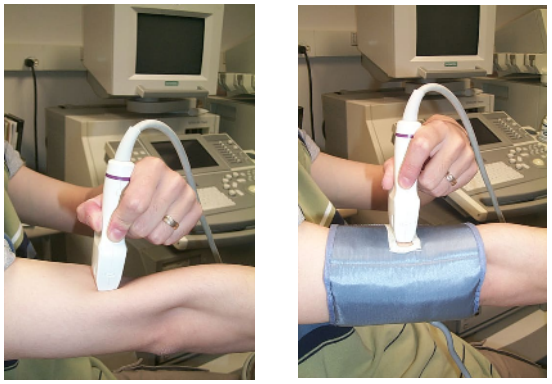

Kim et al, Weitzel et al
University of Michigan
http://bul.eecs.umich.edu/

90

Clinical Data: 5 healthy, 5 diseased arteries

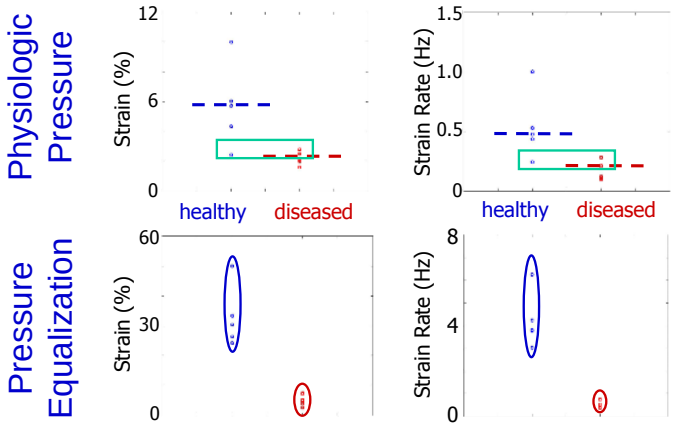

Kim et al, Weitzel et al

91

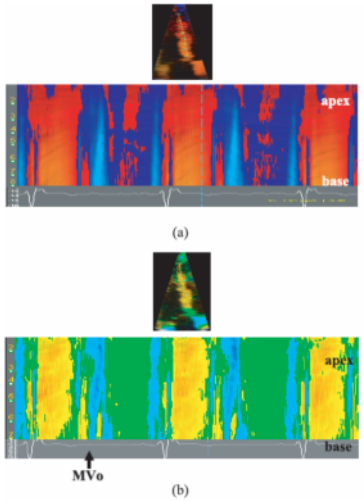

Figure 11. Example of a curved M-mode velocity (a) and strain rate (b) image of a normal volunteer: the velocity or strain rate information of all points along a manually indicated curve on the image, is colour coded and shown as a function of time.

Cardiac Strain and Strain Rate Imaging

- Cross-correlation method
  - high sensitivity
  - high accuracy
  - 2-D or 2.5-D
  - computationally intensive
- Gradient velocity method
  - fast
  - 1-D (axial)
  - aliasing
- Real-time implementation is required

D'hooge et al. 2000

92

Cardiac Strain and Strain Rate Imaging

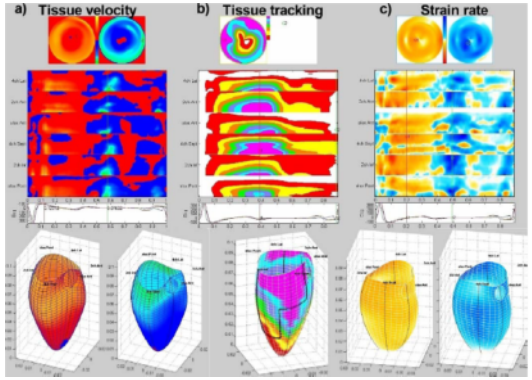

Different parametric imaging in 3-/4D display, all from a normal subject. Left to right: The red-blue display of tissue velocity, the colored bands of tissue tracking and the yellow-blue display of strain rate. In tissue velocity, lighter color represents higher velocities, showing clearly the velocity gradient from base to apex both in systole and diastole. In tissue tracking, each color represents an interval of 2 mm displacement, as shown by the legend. This means that red represents 2 – 4 mm displacement, increasing to magenta showing >14 mm at the base. Strain rate shows shortening in yellow to red, lengthening in blue, darker color represents more deformation. Some inhomogeneity is visible due to noise and dropouts. Top to bottom: Bull's eye display both in systole and diastole (except tissue tracking), M-mode array from all six walls with apex on top and base at the bottom with ECG and a 3D surface reconstruction, velocity and strain rate in systole and diastole. The bull's eye projection shows all of the surface, but the area is distorted; the apex is progressively diminished, while the base is over-represented, the 3D figure shows a representation of the true area, but has to be rotated to see all of the surface. Reconstruction is done from three separate cine-loops, synchronized by means of ECG. The ECG at the left is inverted, but is from the same patient, as may be seen by the end of the cycle, where there is noise in the ECG signal. The aortic annulus and location of the imaging planes are added for orientation.

Støylen, 2003

93

Deep Vein Thrombosis (DVT) and Pulmonary Embolism (PE)

94

Triplex Ultrasound: Grayscale, Doppler, Elasticity

- Sprague-Dawley rats (300 g)
- Surgically induced clots in IVC
- Imaging studies clots at
  - 2-day (acute)
  - 6-day (sub-acute)
  - 9-day (chronic)
- Siemens Sonoline Elegra
  - 9-13 MHz center frequency
- 2-D correlation and strain imaging

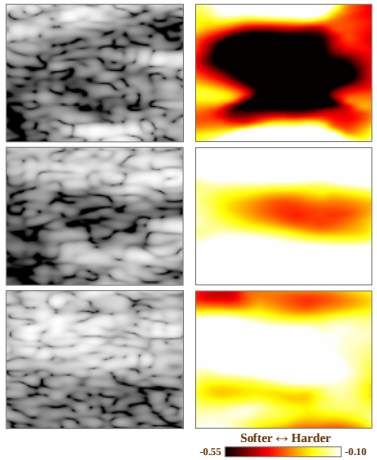

Emelianov, Rubin et al, 2000 and 2002

95

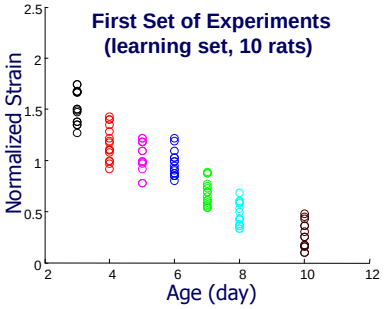

- Fitting of data from the first set of experiments
  $\varepsilon = e^{(aD+b)}$
  ε – normalized strain
  D – age of the clot (day)
- Can first data set predict the age of the clot in the second set of experiments ?

Xie et al 2004

Can elasticity imaging age DVT ?

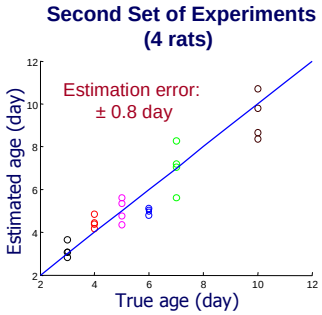

96

Elasticity Imaging to Age DVT

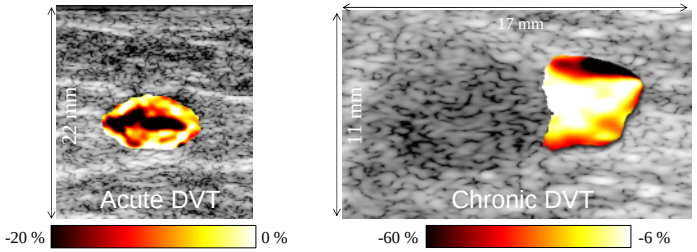

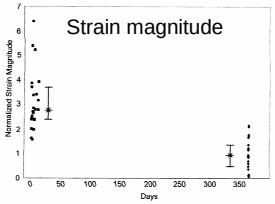

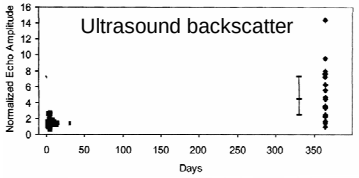

Rubin et al., 2006

3-D Strain Imaging

- Deformation → 3-D motion
- Ultrasound imaging: 2-D
- 3-D tracking is needed
- Results:
  - 2-D linear array
  - Siemens Antares
  - 5:1 contrast
  - 1.5% deformation

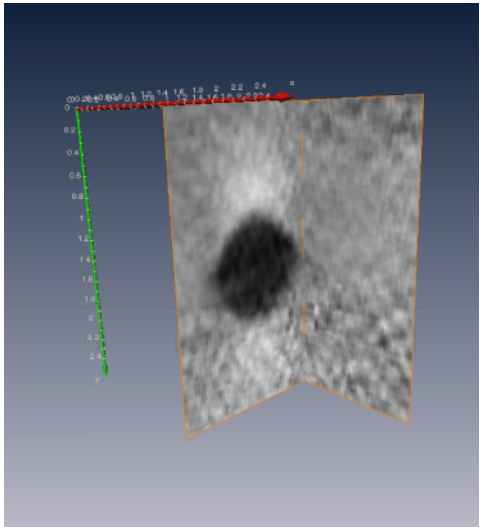

Hall et al, 2006

98

3-D Strain Imaging

- Deformation → 3-D motion
- Ultrasound imaging: 2-D
- 3-D tracking is needed
- Results:
  - 2-D linear array
  - Siemens Antares
  - 5:1 contrast
  - 1.5% deformation

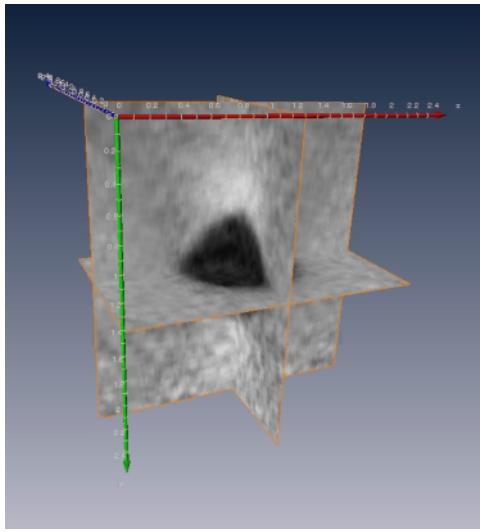

Hall et al, 2006

99

Non-linearity in stress-strain relations

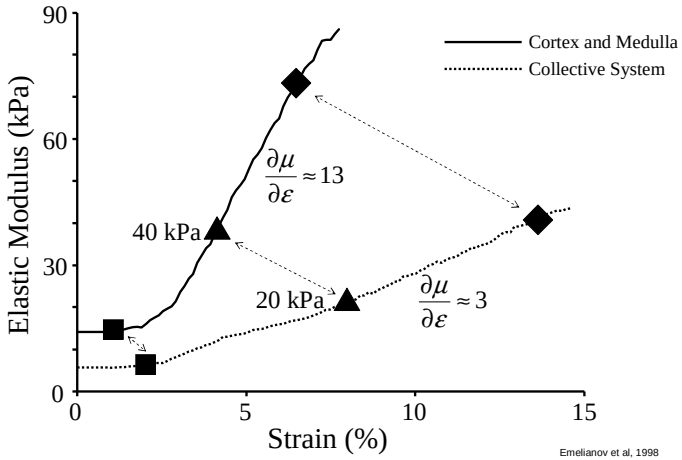

Emelianov et al, 1998
Erkamp et al, 1998, 1999

100

Imaging of Tissue Non-linearity

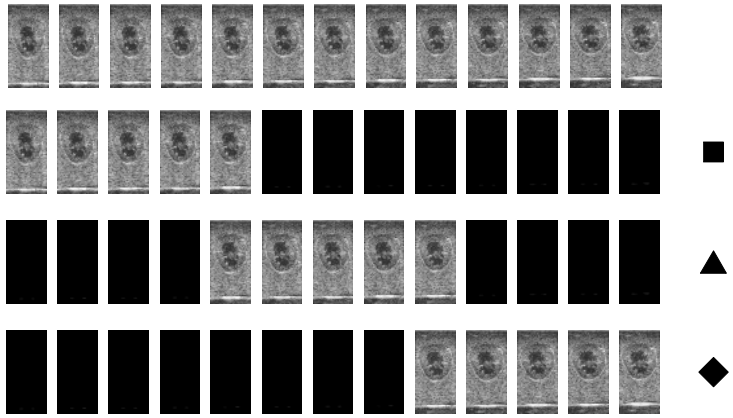

Emelianov et al, 1997
Erkamp et al, 1999

101

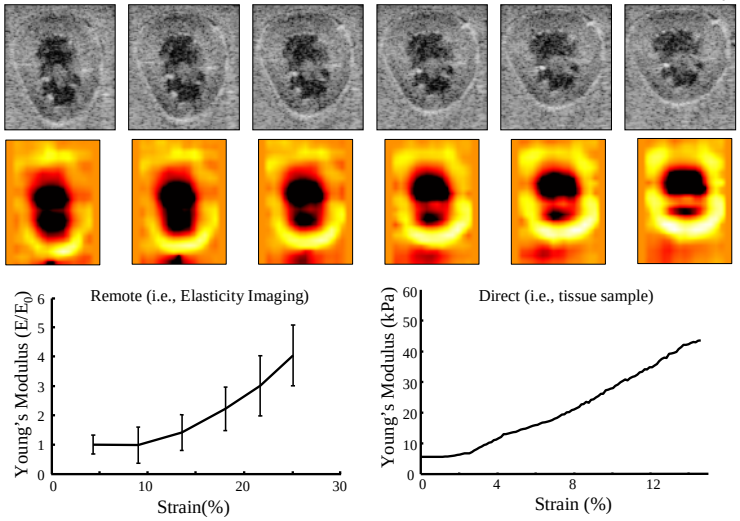

Emelianov et al, 1997; Erkamp et al, 1998

102

Viscoelasticity Imaging

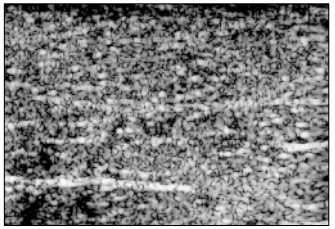

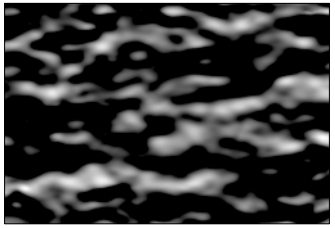

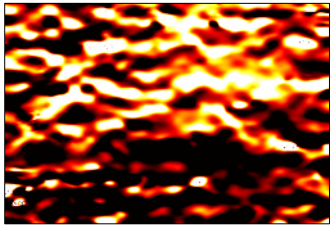

Strain ↔ Elasticity

Creep ↔ Viscosity

103

Retardance Time Imaging, T_1

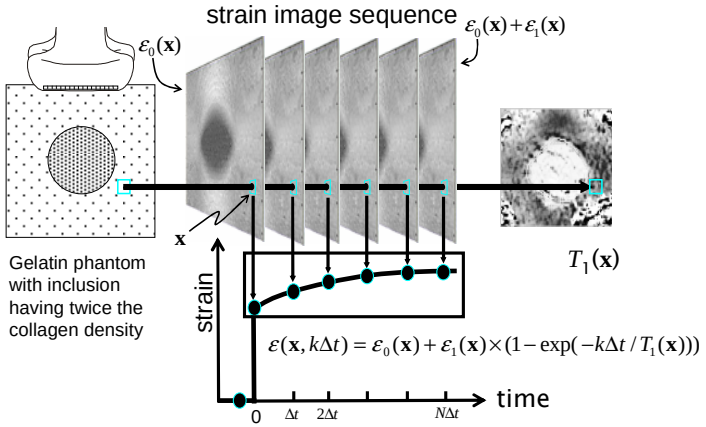

Gelatin phantom with inclusion having twice the collagen density

Michael F. Insana et al. University of Illinois at Urbana-Champaign
http://ultrasonics.bioen.uiuc.edu

104

In Vivo Patient Studies

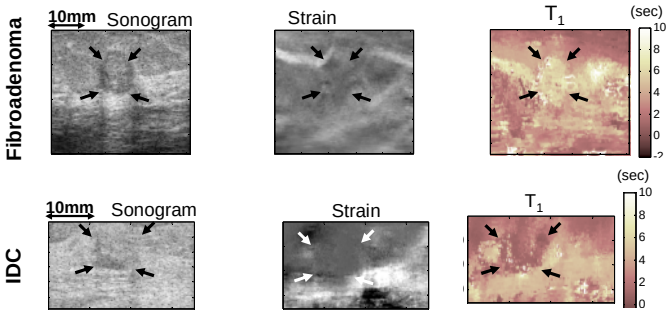

Two patients with 1-cm, non-palpable lesions detected mammographically. With the retardance time image, malignant and benign lesions can be differentiated because of differences in the collagen ultrastructure between the two lesion types.

Sridhar M, Liu J, Insana MF, "Elasticity imaging of polymeric media," *ASME J Biomechan Eng* (in press)

Insana MF, Pellot-Barakat C, Sridhar M, Lindfors K, "Viscoelastic imaging of breast tumor microenvironment with ultrasound," *J Mammary Gland Biol Neoplasia*. 9: 393-404, 2004

Insana MF, "Elasticity imaging," In: *Wiley Encyclopedia of Biomedical Engineering*, M Akay, ed., ISBN: 0-471-24967-X, Hoboken: John Wiley & Sons, Inc., 2006

Acknowledgements

All who contributed to
the field of Elasticity Imaging and
to this presentation